Bulletin of Electrical Engineering and Informatics
Vol. 15, No. 3, June 2026, pp. 1972~1983
ISSN: 2302-9285, DOI: 10.11591/eei.v15i3.11686

MPPT controller for a solar PV array with temperature-compensated P&O algorithm

Abdulaziz H. Yusuf[1], Ceyda Aksoy Tırmıkçı[1], Eltahir Idris Eltahir Mohamed[2]
[1]Department of Electrical and Electronics Engineering, Faculty of Engineering, Sakarya University, Serdivan, Turkey
[2]Department of Information Systems and Technology, Faculty of Computer and Information Sciences, Sakarya University, Serdivan, Turkey

Article Info

Article history:

Received Oct 21, 2025
Revised Mar 18, 2026
Accepted Apr 18, 2026

Keywords:

Boost converter
Maximum power point tracking
Perturb-and-observe algorithm
Photovoltaic systems
Solar power

ABSTRACT

Photovoltaic (PV) systems must operate at the maximum power point (MPP) to maintain efficiency under varying environmental conditions. This study develops a temperature-compensated perturb-and-observe (P&O), maximum power point tracking (MPPT) controller integrated with a boost converter in MATLAB. A 100 kW PV array was modeled using realistic module parameters; baseline experiments without MPPT revealed power losses up to 70% and incorrect power–temperature correlations due to fixed-duty cycle operation. With MPPT enabled, the controller dynamically adjusted the duty ratio, achieving proportional scaling with irradiance and an inversely proportional response to temperature. Results confirm a peak summer output of 48.78 kW compared to 15 kW without MPPT, improving annual energy yield by a factor of three under realistic Sakarya operating conditions.

Corresponding Author:

Eltahir Idris Eltahir Mohamed
Department of Information Systems and Technology, Faculty of Computer and Information Sciences
Sakarya University
Serdivan, Sakarya, Turkey
Email: eltahirmohamed@sakarya.edu.tr

1. INTRODUCTION

Photovoltaic (PV) systems are central to renewable energy due to scalability, low maintenance, and environmental benefits. Efficient operation requires continuous tracking of the maximum power point (MPP). Among maximum power point tracking (MPPT) methods, perturb-and-observe (P&O), and incremental conductance (INC) are widely applied for their simplicity and effectiveness [1], with comparative studies reinforcing their relevance [2]. MPPT controllers, typically implemented with boost converters, adapt to irradiance, temperature, and shading variations [3], as described in foundational power electronics literature [4]. Grid-connected PV systems must comply with interconnection standards covering voltage, frequency, disturbance response, and protection requirements, and simulation-based validation is commonly used to verify both efficiency and safe grid integration [5]. Subsequent research introduced adaptive approaches and detailed PV modeling, highlighting energy-yield improvements and the influence of parasitic resistances in direct current (DC-DC) converters [6]. Recent work emphasizes MPPT integration with boost converters and microcontroller platforms for stable and rapid tracking, including transient analysis of converter signals [3], [6], [7]. MATLAB/Simulink remains a standard environment for MPPT modeling and evaluation [8]. Early comparisons of P&O and INC clarified trade-offs among simplicity, accuracy, and response time [9], while further studies detailed P&O implementation in applications such as PV pumping [10]. Environmental conditions significantly affect PV and MPPT performance. Increased irradiance raises photocurrent, whereas higher temperature reduces open-circuit voltage and shifts the MPP. Accurate PV–converter modeling under

varying conditions, including detailed PV array simulation, is therefore essential. Under partial shading, multiple local maxima require controllers capable of identifying the global MPP [11]. Step-size selection introduces a convergence–stability trade-off, addressed by variable step-size INC methods that adapt to voltage or power variations [12]. Temperature-compensated algorithms further improve tracking accuracy, as shown in comparative studies for battery-charging systems [13]. Detailed PV array models incorporating electrical and thermal parameters support DC-stage analysis in grid-connected systems [14], while integration with battery storage enhances reliability under fluctuating irradiance [15]. Comparative investigations of classical and intelligent MPPT strategies including P&O, FLC, and adaptive neuro-fuzzy inference systems illustrate the growing role of soft-computing and simulation-based benchmarking [16]. Nevertheless, despite extensive research on P&O and temperature effects, few studies integrate temperature compensation directly within the P&O loop using realistic parameters and regional case studies. The need for reliable modeling is further supported by converter comparisons [3], [6], [7] and analyses of irradiance and temperature impacts [17], [18], while recent optimization techniques improve convergence under fast-varying loads and partial shading [19]–[21].

Conventional P&O algorithms are valued for their simplicity but often exhibit steady-state oscillations and neglect the reduction of open-circuit voltage under thermal stress. Although adaptive and soft-computing MPPT methods address these limitations, they typically increase computational complexity. The novelty of this study is the integration of a computationally lightweight temperature-compensation mechanism within the standard P&O loop. Moreover, limited research examines the statistical reliability and long-term stability of P&O controllers under localized meteorological conditions, with many studies overlooking oscillatory behavior during seasonal transitions [22]. The contribution of this work is presenting a year-long, high-resolution statistical evaluation of MPPT performance for the Sakarya region using real meteorological data. A temperature-compensated P&O MPPT model was developed in MATLAB/Simulink and validated with annual climatic data from Sakarya to assess tracking efficiency and energy yield under realistic conditions.

2. EXPERIMENTAL SETUP

The PV module produces an output voltage (V_{PV}) and current (I_{PV}) corresponding to the incident solar irradiance (I_r). These outputs are supplied to the MPPT controller, which also receives temperature (T) as an input to compensate for temperature-dependent variations in PV performance. The MPPT controller processes these input signals and generates a pulse-width modulation (PWM) control signal used to drive the boost converter. The boost converter then increases the PV voltage to the desired level, and the regulated output is delivered to a 2 Ω load. The block diagram of this is illustrated in Figure 1.

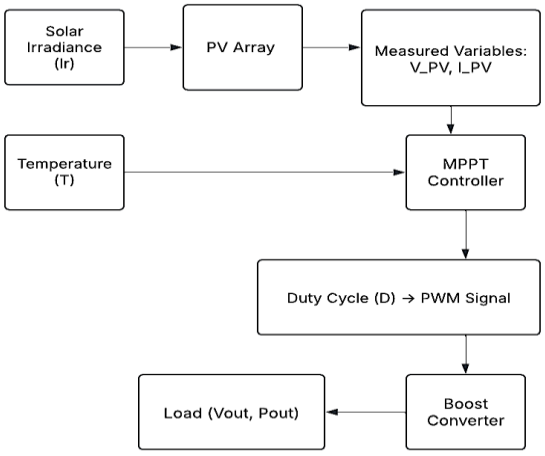

Figure 1. Block diagram of the PV–boost converter with MPPT control, showing irradiance and temperature inputs, PV measurements, PWM signal, and load outputs (Vout and Pout)

The PV-boost converter system is defined by the electrical parameters of the array and converter. The array comprises 10 series-connected modules per string and 47 parallel strings, yielding a total maximum power of 213.15 W per module STC. Each module has an open-circuit voltage of 36.3 V, a MPP voltage of 29 V, an MPP current of 7.35 A, and a short-circuit current of 7.84 A. Temperature effects are captured by a

–0.3609 %/°C coefficient for open-circuit voltage and a +0.102 %/°C coefficient for short-circuit current [8]. The boost converter steps the PV input voltage (250–350 V) to a regulated 600 V DC output. The configuration of the system is presented in Figure 2.

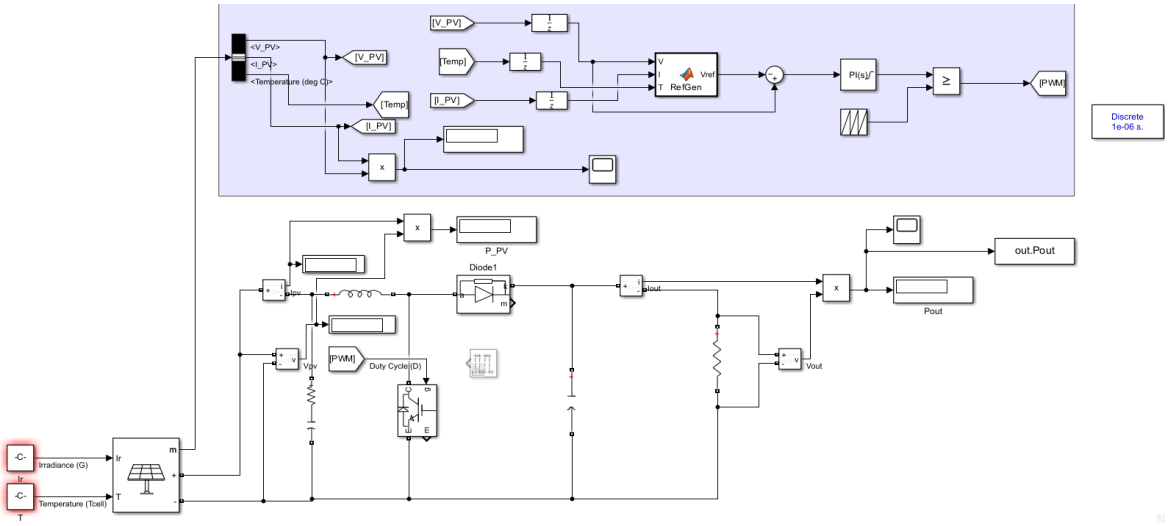

Figure 2. Simulink implementation of the PV–boost converter with MPPT controller, showing labeled inputs (irradiance and temperature), measured signals (Vpv, Ipv, Iout, Vout, and Pout), and control path (duty cycle)

The PV array serves as the system input, configured with 10 modules in series per string and 47 strings in parallel, giving a total of 470 modules. Each module operates at 29 V and 7.35 A at its MPP, yielding 213.15 W. STC (1000 W/m² irradiance, 25 °C cell temperature), the complete array delivers approximately 100 kW. The open-circuit voltage temperature coefficient is −0.3609 %/°C per module, meaning array voltage decreases with increasing temperature, motivating the integration of temperature compensation within the MPPT controller [8]. The switching frequency is set to 66.7 kHz, balancing efficiency and component sizing. In continuous conduction mode, the duty cycle is given by [4]:

$$D = 1 - \frac{V_{in}}{V_{out}} \tag{1}$$

Where D is the converter duty cycle, V_{in} is the input PV voltage, and V_{out} is the regulated output voltage.

For example, at V_{in}=250 V, the duty cycle is: $D = 1 - \frac{250}{600} = 0.5833$.

At rated power (100 kW), the input current is:

$$\mathrm{I_{in}} = \frac{\mathrm{P}}{\mathrm{V_{in}}} = \frac{100000}{250} = 400\ \mathrm{A} \tag{2}$$

Where $\mathrm{I_{in}}$ represents the input current and P is the array power.
With ripple limited to 5% of input current ($\Delta \mathrm{I_L} = 20$ A), the inductance is [4].

$$L = \frac{V_{in} \times D}{\Delta I_L \times f_s} \tag{3}$$

Where L is the required boost inductance, ΔI_L is the inductor current ripple, and f_s is the switching frequency.

At $V_{in} = 250$ V, $D = 0.5833$, $\Delta I_L = 20$ A, $f_s = 66.7$ kHz: $L = \frac{250 \times 0.5833}{20 \times 66.7 \times 10^3} \approx 1.458$ mH

At $V_{in} = 350$ V, $D = 0.4167$, $\Delta I_L = 14.3$ A, $f_s = 66.7$ kHz: $L = \frac{350 \times 0.4167}{14.3 \times 66.7 \times 10^3} \approx 2.042$ mH

Selected design value:

$L = 1.45$ mH

The output capacitor is sized to keep voltage ripple below 1% ($\Delta V = 6$ V) [4]:

$$C = \frac{I_{out} \times D}{\Delta V \times f_s} \quad (4)$$

Where C is the output capacitance, ΔV is the maximum voltage ripple, and I_{out} is the output load current. The output current is:

$$I_{out} = \frac{P}{V_{out}} \quad (5)$$

At $V_{in} = 250$ V, $D = 0.5833$, $I_{out} = 166.7$ A, $\Delta V = 6$ V, $f_s = 66.7$ kHz:
$C = \frac{166.7 \times 0.5833}{6 \times 66.7 \times 10^3} \approx 3.24$ mF

At $V_{in} = 350$ V, $D = 0.4167$, $I_{out} = 166.7$ A, $\Delta V = 6$ V, $f_s = 66.7$ kHz:
$C = \frac{166.7 \times 0.4167}{6 \times 66.7 \times 10^3} \approx 2.31$ mF

Selected design value:

$C = 3.227$ mF

The switching element is an insulated gate bipolar transistor (IGBT) rated for the full 600 V output and peak currents exceeding 400 A. A diode provides the freewheeling path during the IGBT OFF state, enabling stable boost conversion while the MPPT controller adjusts the duty cycle to maintain maximum power extraction [4]. The MPPT control block ensures that the PV array operates at its MPP under varying environmental conditions. It receives PV voltage, current, and temperature as inputs, from which power is calculated and compared with a reference generated by the RefGen unit. The signals are sampled through discrete integrators to estimate the reference voltage, which is then compared with the actual PV voltage. The resulting error is processed by a proportional–integral (PI) controller that regulates the boost converter duty cycle through a PWM generator operating at 66.7 kHz. The controller uses a P&O strategy with temperature compensation. Power variations relative to voltage perturbations determine the perturbation direction: if power decreases, the direction is reversed; if it increases, the reference is maintained. A correction factor derived from the open-circuit voltage temperature coefficient adjusts the reference voltage to account for thermal effects. All experiments were performed in MATLAB/Simulink (R2024b), serving as a virtual laboratory environment. A variable-step ode23t (modified stiff/Trapezoidal) solver was used to manage stiff switching dynamics, with a relative tolerance of 1e-3 and a fixed sampling time of 1 µs to resolve high-frequency behavior. Each monthly simulation ran for 0.5 s (500,000 iterations). The PV system was modeled using the Simscape electrical PV array block, and the boost converter was constructed with discrete components (inductor, IGBT, diode, and capacitor) operating at 66.7 kHz, controlled either by fixed-duty PWM or the MPPT algorithm. As a baseline, the converter was tested without MPPT using a fixed 53% duty cycle at 66.7 kHz. Two experiments were performed: a temperature sweep from 5 °C to 45 °C in 10 °C steps at constant irradiance (1000 W/m²), and an irradiance sweep from 200 to 1000 W/m² in 200 W/m² increments at constant temperature (25 °C). Output power was recorded to capture both transient and steady-state behavior. The same experiments were then repeated with the MPPT controller enabled. The choice of 25 °C as reference reflects the adopted STC, under which PV modules are rated in both research and industry [23]. Table 1 provides a summary of the PV array specifications as well as the boost converter's parameters.

Table 1. PV array and converter parameters

Parameter	Value
PV array rated power	100 kW
Parallel strings	47
Series modules per string	10
Cells per module	60
Open-circuit voltage (V_{oc})	36.3 V
Short-circuit current (I_{sc})	7.84 A
Boost inductor (L)	1.45 mH
Output capacitor (C)	3.227 mF
Switch	IGBT+freewheeling diode
Switching frequency	66.7 kHz
Sampling time	1 µs
Outputs	Vout and Pout

Table 2 summarizes the seasonal meteorological profile of Sakarya across a full year, detailing the average monthly temperature, daylength, and solar irradiance (GHI) metrics that serve as the environmental operating conditions for the system.

Table 2. Average monthly temperature and irradiance in Sakarya

Month	Temp (°C)	Daylength at 15th (in hours)	Monthly GHI (kWh/m²)	Monthly average daylight GHI (W/m²)
January	6.4	9:40	57.48	191.8131
February	7.1	10:42	66.11	220.6609
March	9.3	11:56	82.20	222.2022
April	13.2	13:15	119.47	300.5535
May	17.9	14:21	126.19	283.6687
June	22.1	14:56	169.15	377.5670
July	24.3	14:40	219.25	482.2214
August	24.4	13:42	180.25	424.4172
September	20.6	12:26	148.09	397.0241
October	16.4	11:10	99.77	288.2138
November	12.0	10:00	51.31	171.0333
December	8.3	9:23	52.46	180.3472

To derive the monthly average daylight GHI values shown in Table 2, a two-step procedure was applied. First, the monthly global horizontal irradiation (H_m, in kWh/m²), and average temperatures were obtained for Sakarya [24]-[26]. This represents the total solar energy received over an entire month. The average daily irradiation was calculated as $\frac{Hm}{N_d}$, where N_d is the number of days per month. Next (G_{avg}, in W/m²) was determined by $\frac{H_d \times 1000}{t_{dl}}$, normalizing daily energy against the daylength (t_{dl}) at the 15th day of each month. This method provides a normalized power density that accounts for seasonal variation in daylight hours.

3. RESULTS AND DISCUSSIONS

To obtain the results of the PV-boost converter system under varying irradiance and temperature conditions, the baseline case without MPPT is analyzed to highlight the limitations of fixed-duty operation. Then, the performance with the proposed MPPT controller is examined, showing improvements in steady-state tracking, dynamic response, and energy yield.

3.1. Results without maximum power point tracking

Figures 3 and 4 illustrate the baseline transient and steady-state performance of the PV array operating with a fixed duty cycle (without active MPPT control) under varying environmental conditions. While Figure 4 demonstrates that output power scales proportionally with irradiance, ranging broadly from approximately 2 kW at 200 W/m² to 68 kW at 1000 W/m², Figure 3 exposes a critical flaw in fixed-duty operation.

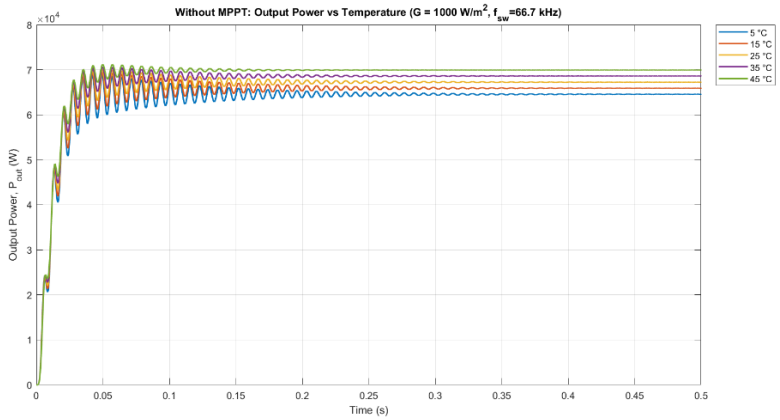

Figure 3. Output power in W vs time in seconds under varying temperatures in °C with MPPT disabled

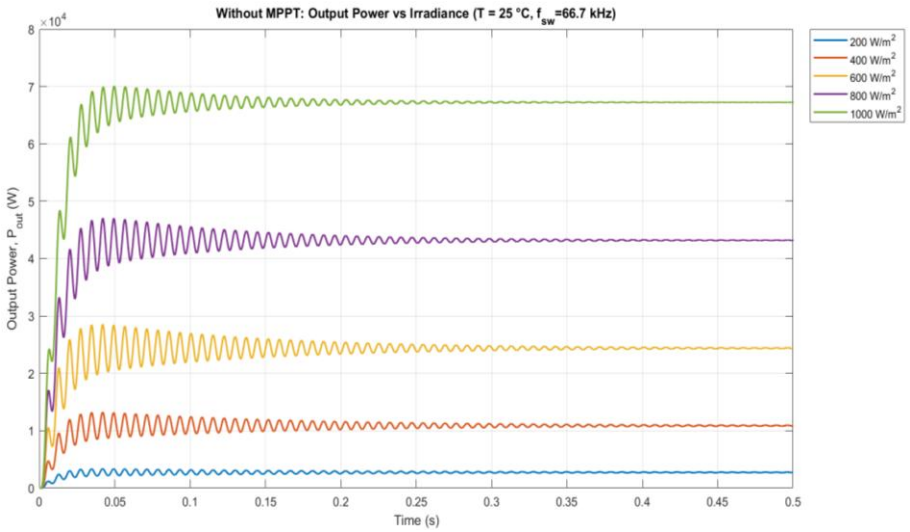

Figure 4. Output power in W vs time in seconds under varying irradiance values in W/m² with MPPT disabled

Specifically, the temperature sweep from 5 °C to 45 °C results in a tightly clustered output where power artificially increases with temperature, peaking near 70 kW at 45 °C. This misleading positive correlation fundamentally contradicts the established physical behavior of PV cells, wherein energy conversion efficiency inherently degrades as cell temperature rises. Consequently, these baseline findings confirm that a fixed-duty approach forces the system to operate far from its true MPP, thereby inducing false performance trends and validating the absolute necessity of the proposed P&O controller for accurate, physics-compliant energy extraction.

3.2. Results with maximum power point tracking

As observed in Figure 5, the MPPT controller successfully corrects the artificial positive correlation seen in the unoptimized system; as the cell temperature increases from 5 °C to 45 °C, the tracked steady-state output power accurately decreases from over 100 kW to approximately 70 kW. This inversely proportional response perfectly aligns with established PV semiconductor theories, demonstrating that the controller correctly accounts for the degradation of open-circuit voltage under elevated thermal conditions.

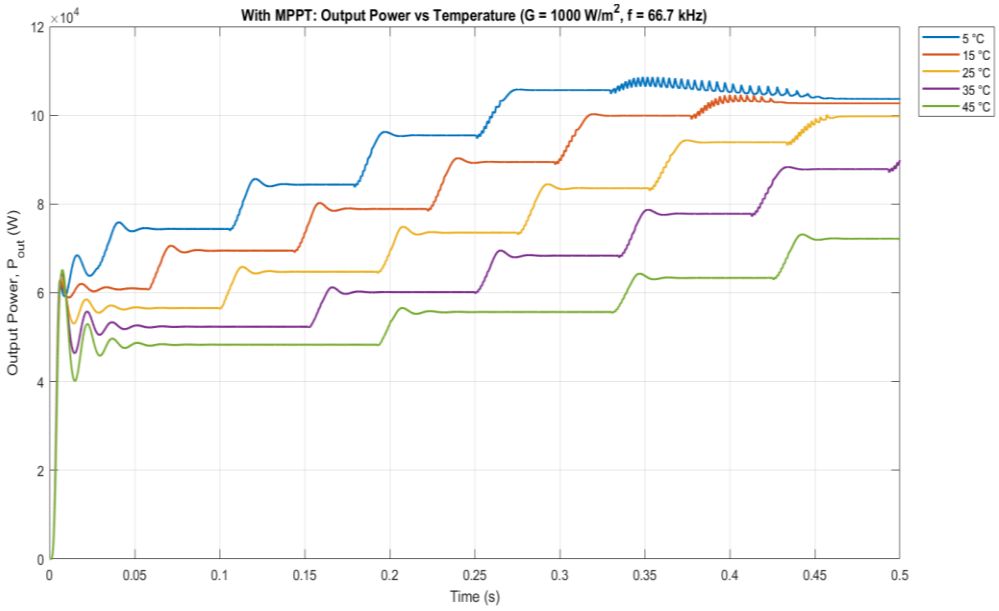

Figure 5. Output power in W vs time in seconds under varying temperatures in °C with MPPT enabled

Conversely, Figure 6 confirms the system's ability to scale energy extraction proportionally with solar availability, successfully tracking the theoretical MPP from approximately 10 kW at 200 W/m² up to the peak 100 kW at 1000 W/m². Crucially, both scenarios reveal the characteristic transient and steady-state dynamics of the P&O algorithm. The curves display a distinct step-wise search phase during the initial transient period (0 to 0.45 s) as the algorithm rapidly climbs the power curve. Once convergence is achieved, the controller settles into continuous, small-amplitude steady-state oscillations. As supported by previous literature, these localized perturbations (approximately ±1–2%) are the necessary tradeoff of the P&O method.

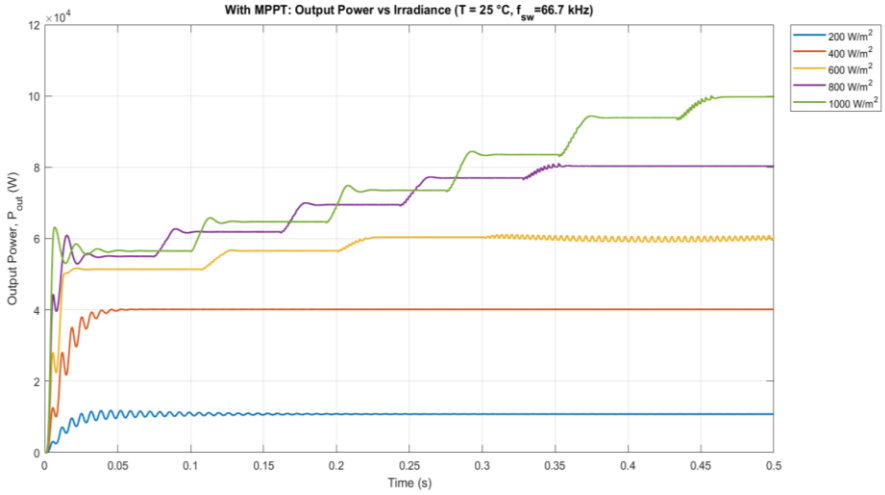

Figure 6. Output power in W vs time in seconds under varying irradiance values in W/m² with MPPT

3.3. Comparison of the results

Figures 7 and 8 present a comparative steady-state analysis of the active MPPT controller against an unoptimized fixed-duty baseline. The temperature sweep shown in Figure 7 exposes a fundamental failure in the open-loop system: where power increases (from approximately 64.5 kW to 70 kW) under rising thermal stress. The active MPPT corrects this anomaly, enforcing a physically valid, inversely proportional degradation (from ~104 kW to 72 kW) that aligns precisely with established PV semiconductor thermodynamics. Furthermore, Figure 8 confirms the controller's optimal extraction capability by maintaining strict linear proportionality up to the theoretical array limit of 100 kW, whereas the baseline suffers non-linear degradation capped at ~67 kW. The widening energy gap between these trajectories visualizes the recovered power, proving that the P&O algorithm guarantees maximum theoretical energy yields across all boundary conditions.

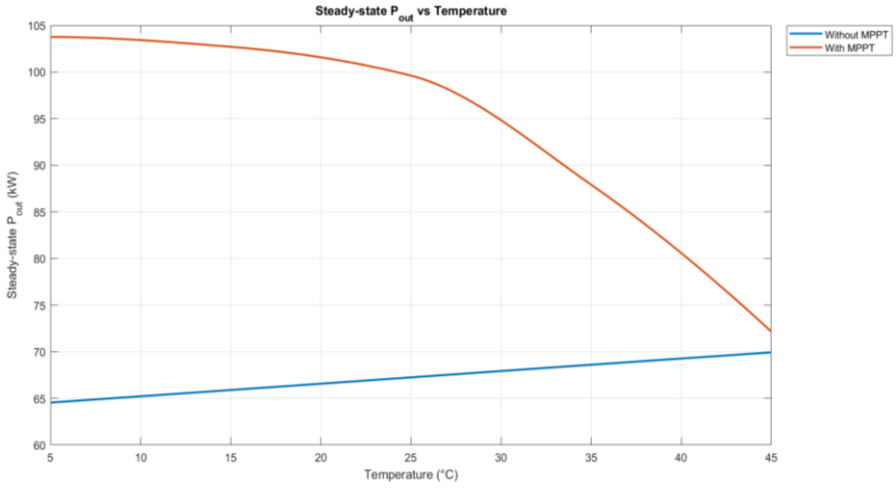

Figure 7. Steady-state output power in kW vs temperature in °C with MPPT in red and without MPPT in blue

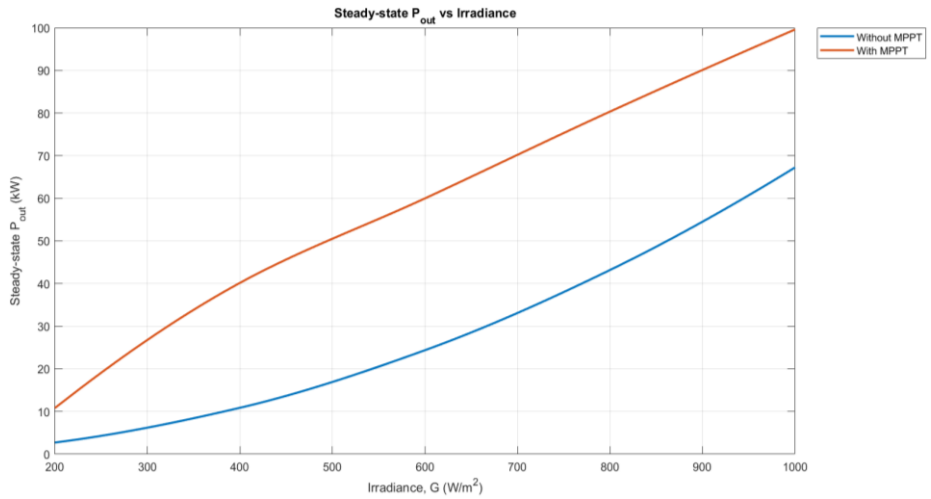

Figure 8. Steady-state output power vs irradiance ranging from 200 to 1000 W/m² MPPT in red and without MPPT in blue

Figure 9 presents a comparison of steady-state output power in Sakarya, demonstrating the contribution of the active MPPT controller under real meteorological conditions. Both trajectories follow the region's seasonal solar profile; however, the performance difference is substantial. The active MPPT tracks the MPP across seasonal transitions and reaches a peak summer output of 48.78 kW, while the fixed-duty baseline experiences static impedance mismatch and is limited to approximately 15 kW. The large area between the curves represents the recovered annual energy, showing that dynamic P&O optimization is necessary to overcome thermal and irradiance variations and maintain maximum energy yield throughout the year.

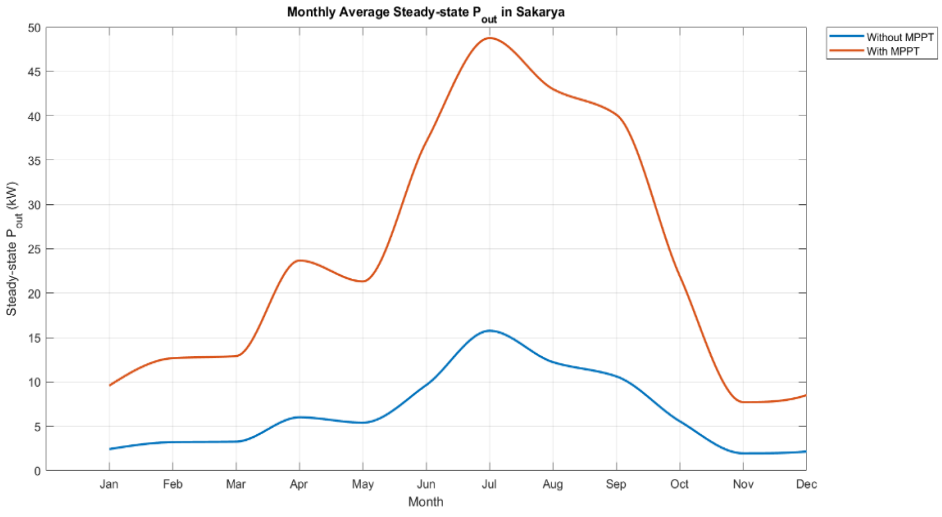

Figure 9. Average monthly steady-state output power in Sakarya

Table 3 details the steady-state performance of the P&O MPPT controller across irradiance levels from 200 to 1000 W/m². The algorithm demonstrates high precision, closely tracking the linearly scaling theoretical MPP. Efficiency starts at 91.9% at 200 W/m² (10.81 kW extracted versus 10 kW theoretical) but rapidly approaches near-ideal performance, consistently exceeding 98.9% for all irradiances above 200 W/m² (e.g., 99.61% at 800 W/m²). To minimize steady-state losses, the P&O algorithm continuously perturbs the duty ratio, resulting in minor, inherent oscillations (±1–2% amplitude) governed by the 1 µs sample time and 66.7 kHz converter switching frequency. While slightly reducing instantaneous efficiency at the lowest

irradiance levels, these perturbations guarantee rapid convergence and robust tracking under dynamic environmental conditions.

Table 3. Steady-state MPPT performance under different irradiance levels in W/m², at 25 °C

Irradiance (W/m²)	Theoretical MPP (kW)	Tracked power (kW)	Tracking efficiency η_{mppt} (%)
200	10	10.81	91.9
400	40	40.17	99.575
600	60	60.64	98.933
800	80	80.31	99.6125
1000	100	99.72	99.72

To derive the statistical validation presented in Figure 10, the simulation was executed for a duration of 0.5 s. To isolate the true operational stability from start-up transients, the output data was sampled from a defined steady-state analysis window spanning from 0.45 s to 0.5 s. Within this high-resolution temporal boundary, the mean steady-state output power μ and its corresponding standard deviation σ were computed to quantify the performance metrics. The resulting visualization confirms the annual operational stability of the MPPT controller under realistic, fluctuating environmental conditions. The system effectively tracks the region's seasonal solar trajectory, achieving a maximum mean output of 48.78 kW in July, corresponding with peak regional insolation, and a minimum of 7.71 kW during the reduced irradiance of November.

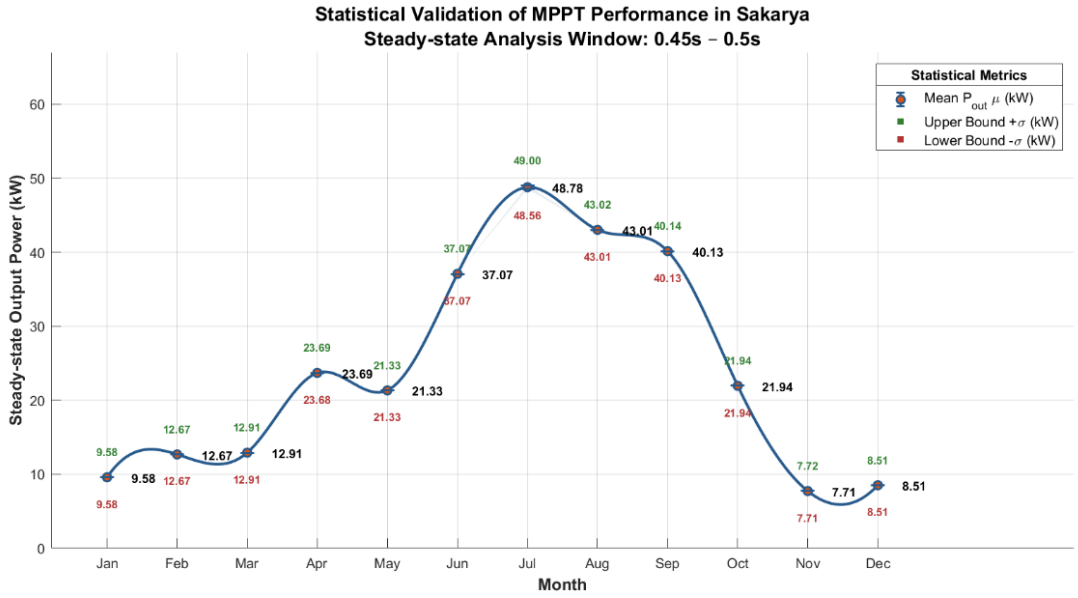

Figure 10. Means and standard deviations of steady-state output power in kW

To clearly define the position and contribution of this work within the existing literature, Table 4 presents a comparative performance analysis of the proposed method against established MPPT techniques. Most studies evaluate MPPT controllers under STC and short-term transients [22], [27]. In contrast, this work uses continuous operational sweeps and localized meteorological data from Sakarya. By applying statistical validation based on steady-state mean power and standard deviation, the study distinguishes true algorithmic stability from numerical artifacts and demonstrates reliable tracking performance under realistic conditions [28]. The proposed controller also corrects the artificial positive power–temperature correlation observed in open-loop systems and maintains physically accurate energy extraction under thermal stress. In the Sakarya case, tracking efficiency remains above 98.9%, indicating that temperature compensation mitigates thermally induced voltage drops and improves the energy yield and reliability of practical PV installations.

Table 4. Comparison between the proposed method and established MPPT techniques

MPPT algorithm	Tracking efficiency %	Convergence speed	Implementation complexity
Conventional P&O	Medium ~95	Moderate/slow	Low
INC	High ~98	Moderate	Medium
Fuzzy logic	Very high >99	Fast	High
Proposed temp-comp P&O	High >98.9	Fast	Low-medium

4. CONCLUSION

The results quantitatively demonstrate that fixed-duty-cycle operation significantly restricts energy harvesting capability. In contrast, the proposed MPPT controller successfully tracked the MPP, consistently achieving a tracking efficiency exceeding 98.9% across irradiance levels from 400 to 1000 W/m^2. A substantial improvement in energy yield was confirmed in the Sakarya case study, where peak summer output reached 48.78 (±0.22) kW using MPPT, compared to only 15 kW without MPPT. These findings emphasize the necessity of adaptive MPPT strategies to maximize PV system efficiency. Future work may extend this research through experimental hardware validation, and evaluating the controller under rapid irradiance variations, such as fast-moving cloud transients, and complex partial shading scenarios. Additionally, experimental hardware validation using a rapid prototyping microcontroller platform will be conducted to assess real-time execution and compare the controller's performance against advanced soft-computing and intelligent MPPT techniques.

ACKNOWLEDGMENTS

The authors thank Sakarya University for providing the environment necessary for the completion of this study.

FUNDING INFORMATION

This research did not receive any specific grant from funding agencies.

AUTHOR CONTRIBUTIONS STATEMENT

This journal uses the Contributor Roles Taxonomy (CRediT) to recognize individual author contributions, reduce authorship disputes, and facilitate collaboration.

Name of Author	C	M	So	Va	Fo	I	R	D	O	E	Vi	Su	P	Fu
Abdulaziz H. Yusuf	✓	✓	✓					✓	✓	✓	✓			
Ceyda Aksoy Tırmıkçı	✓		✓	✓	✓	✓	✓	✓		✓	✓	✓	✓	
Eltahir Idris Eltahir Mohamed	✓	✓		✓	✓	✓	✓		✓	✓		✓		

C : **C**onceptualization
M : **M**ethodology
So : **So**ftware
Va : **Va**lidation
Fo : **Fo**rmal analysis
I : **I**nvestigation
R : **R**esources
D : **D**ata Curation
O : Writing - **O**riginal Draft
E : Writing - Review & **E**diting
Vi : **Vi**sualization
Su : **Su**pervision
P : **P**roject administration
Fu : **Fu**nding acquisition

CONFLICT OF INTEREST STATEMENT

The authors declare no conflict of interest.

DATA AVAILABILITY

Derived data supporting the findings of this study are available from the corresponding author [E. I. Eltahir] upon request.

REFERENCES

[1] T. Esram and P. L. Chapman, "Comparison of photovoltaic array maximum power point tracking techniques," *IEEE Trans. Energy Convers.*, vol. 22, no. 2, pp. 439–449, 2007, doi: 10.1109/TEC.2006.874230.

[2] B. Subudhi and R. Pradhan, "A comparative study on maximum power point tracking techniques for photovoltaic power systems," *IEEE Trans. Sustain. Energy*, vol. 4, no. 1, pp. 89–98, 2013, doi: 10.1109/TSTE.2012.2202294.

[3] E. Koutroulis, K. Kalaitzakis, and N. C. Voulgaris, "Development of a microcontroller-based, photovoltaic maximum power point tracking control system," *IEEE Trans. Power Electron.*, vol. 16, no. 1, pp. 46–54, 2001, doi: 10.1109/63.903988.

[4] R. W. Erickson and D. Maksimovic, "Fundamentals of Power Electronics," 2nd ed. Boston, MA: Springer, 2001.

[5] Institute of Electrical and Electronics Engineers, "IEEE Standard for Interconnection and Interoperability of Distributed Energy Resources with Associated Electric Power Systems Interfaces," *IEEE Std 1547-2018 (Revision IEEE Std 1547-2003)*, no. February, pp. 1–138, 2018, doi: 10.1109/IEEESTD.2018.8332112.

[6] M. Walczak and L. Bychto, "Influence of parasitic resistances on the input resistance of buck and boost converters in maximum power point tracking (Mppt) systems," *Electron.*, vol. 10, no. 12, 2021, doi: 10.3390/electronics10121464.

[7] M. Walczak and L. Bychto, "Transients in Input and Output Signals in DC–DC Converters Working in Maximum Power Point Tracking Systems," *Energies*, vol. 16, no. 12, 2023, doi: 10.3390/en16124565.

[8] MATLAB and Simulink Documentation, MathWorks, 2024. [Online]. Available: https://www.mathworks.com. (Accessed: Sep. 30, 2025).

[9] D. P. Hohm and M. E. Ropp, "Comparative study of maximum power point tracking algorithms," *Prog. Photovoltaics Res. Appl.*, vol. 11, no. 1, pp. 47–62, 2003, doi: 10.1002/pip.459.

[10] M. A. Elgendy, B. Zahawi, and D. J. Atkinson, "Assessment of Perturb and Observe MPPT Algorithm Implementation Techniques for PV Pumping Applications," *IEEE Trans. Sustain. Energy*, vol. 3, no. 1, pp. 21–33, Jan. 2012, doi: 10.1109/TSTE.2011.2168245.

[11] M. G. Villalva, J. R. Gazoli, and E. R. Filho, "Comprehensive Approach to Modeling and Simulation of Photovoltaic Arrays," *IEEE Trans. Power Electron.*, vol. 24, no. 5, pp. 1198–1208, May 2009, doi: 10.1109/TPEL.2009.2013862.

[12] F. Liu, S. Duan, F. Liu, B. Liu, and Y. Kang, "A variable step size INC MPPT method for PV systems," *IEEE Trans. Ind. Electron.*, vol. 55, no. 7, pp. 2622–2628, 2008, doi: 10.1109/TIE.2008.920550.

[13] K. H. Akhil, T. H. Hrithik, N. Mishra, S. Lekshmi, M. R. Rashmi, and H. P. Lee, "Comparison of Performance of MPPT Algorithms for Solar Powered Battery Charging Applications," in *3rd Int. Conf. Adv. Technol. ICONAT 2024*, 2024, doi: 10.1109/ICONAT61936.2024.10775288.

[14] N. Motan, M. Abu-Khaizaran, and M. Quraan, "Photovoltaic Array Modelling and Boost-Converter Controller-Design for a 6kW Grid-Connected Photovoltaic System - DC Stage," in *IEEE Int. Conf. Environ. Electr. Eng. (EEEIC) / IEEE Ind. Commer. Power Syst. Eur. (I&CPS Eur.)*, IEEE, Jun. 2018, pp. 1–6, doi: 10.1109/EEEIC.2018.8494003.

[15] K. C. Divya and J. Østergaard, "Battery energy storage technology for power systems-An overview," *Electr. Power Syst. Res.*, vol. 79, no. 4, pp. 511–520, 2009, doi: 10.1016/j.epsr.2008.09.017.

[16] M. S. Sujatha, S. P. Akkisetti, B. V. S. Thrinath, P. P. Selvam, V. B. Kumar, and B. A. Kumar, "Implementation of Perturb & Observe, FLC and ANFIS MPPT Strategy with Buck and Boost Converters in Photovoltaic Systems," in *Int. Conf. Comput. Innov. Eng. Sustain. ICCIES 2025*, 2025, doi: 10.1109/ICCIES63851.2025.11033058.

[17] A. K. Podder, N. K. Roy, and H. R. Pota, "MPPT methods for solar PV systems: A critical review based on tracking nature," *IET Renew. Power Gener.*, vol. 13, no. 10, pp. 1615–1632, 2019, doi: 10.1049/iet-rpg.2018.5946.

[18] S. H. Hanzaei, S. A. Gorji, and M. Ektesabi, "A scheme-based review of MPPT techniques with respect to input variables including solar irradiance and PV arrays' temperature," *IEEE Access*, vol. 8, pp. 182229–182239, 2020, doi: 10.1109/ACCESS.2020.3028580.

[19] I. Shams, S. Mekhilef, and K. S. Tey, "Improved-Team-Game-Optimization-Algorithm-Based Solar MPPT With Fast Convergence Speed and Fast Response to Load Variations," *IEEE Trans. Ind. Electron.*, vol. 68, no. 8, pp. 7093–7103, Aug. 2021, doi: 10.1109/TIE.2020.3001798.

[20] I. Shams, S. Mekhilef, and K. S. Tey, "Maximum Power Point Tracking Using Modified Butterfly Optimization Algorithm for Partial Shading, Uniform Shading, and Fast Varying Load Conditions," *IEEE Trans. Power Electron.*, vol. 36, no. 5, pp. 5569–5581, 2021, doi: 10.1109/TPEL.2020.3029607.

[21] I. Pervez, I. Shams, S. Mekhilef, A. Sarwar, M. Tariq, and B. Alamri, "Most Valuable Player Algorithm based Maximum Power Point Tracking for a Partially Shaded PV Generation System," *IEEE Trans. Sustain. Energy*, vol. 12, no. 4, pp. 1876-1890, Oct. 2021, doi: 10.1109/TSTE.2021.3069262.

[22] M. S. Endiz, G. Gökkuş, A. E. Coşgun, and H. Demir, "A Review of Traditional and Advanced MPPT Approaches for PV Systems Under Uniformly Insolation and Partially Shaded Conditions," *Appl. Sci.*, vol. 15, no. 3, 2025, doi: 10.3390/app15031031.

[23] M. Steiner and G. Siefer, "Translation of outdoor tandem PV module I–V measurements to a STC power rating," *Prog. Photovoltaics Res. Appl.*, vol. 31, no. 8, pp. 862–869, 2023, doi: 10.1002/pip.3691.

[24] Joint Research Centre, "PV Geographical Information System (PVGIS) - Monthly radiation data API (Sakarya, Turkey," European Commission, 2023. [Online]. Available: https://re.jrc.ec.europa.eu/api/v5_3/MRcalc?lat=40.78&lon=30.41&raddatabase=PVGIS-SARAH3&horirrad=1&outputformat=json&startyear=2023&endyear=2023. (Accessed: Sep. 30, 2025).

[25] Turkish State Meteorological Service (MGM), "Forecast cities — Sakarya," 2025. [Online]. Available: https://www.mgm.gov.tr/eng/forecast-cities.aspx?m=SAKARYA. (Accessed: Sep. 29, 2025).

[26] Timeanddate.com, "Sun & moon — Sakarya (Lat 40.78°N, Lon 30.41°E): April 2024 sunrise, sunset, day length," 2024. [Online]. Available: https://www.timeanddate.com/sun/@302114?month=4&year=2024. (Accessed: Sep. 30, 2025).

[27] M. Y. Worku *et al.*, "A Comprehensive Review of Recent Maximum Power Point Tracking Techniques for Photovoltaic Systems under Partial Shading," *Sustain.*, vol. 15, no. 14, 2023, doi: 10.3390/su151411132.

[28] R. I. Jabbar, S. Mekhilef, M. Mubin, and K. K. Mohammed, "A Modified Perturb and Observe MPPT for a Fast and Accurate Tracking of MPP Under Varying Weather Conditions," *IEEE Access*, vol. 11, pp. 76166–76176, 2023, doi: 10.1109/ACCESS.2023.3297445.

BIOGRAPHIES OF AUTHORS

Abdulaziz H. Yusuf earned his B.Sc. in Electrical and Electronics Engineering from Sakarya University in 2026. His academic work focuses on renewable energy, advanced circuit design, and control systems. He can be contacted at email: abdulaziz.yusuf@ogr.sakarya.edu.tr.

Ceyda Aksoy Tırmıkçı is a faculty member at Sakarya University. She received her Ph.D. in 2018 and specializes in high-efficiency solar energy systems and sustainability. She can be contacted at email: caksoy@sakarya.edu.tr.

Eltahir Idris Eltahir Mohamed is an Assistant Professor at Sakarya University. He received his Ph.D. in Electrical and Electronics Engineering in 2021 and has authored over 15 publications focused on radio link design and RF propagation. He can be contacted at email: eltahirmohamed@sakarya.edu.tr.